Nanoscale Advances

Accepted Manuscript

This article can be cited before page numbers have been issued, to do this please use: A. Darabi, M. Nikoorazm and B. Tahmasbi, *Nanoscale Adv.*, 2026, DOI: 10.1039/D5NA00951K.

ROYAL SOCIETY OF CHEMISTRY

rsc.li/nanoscale-advances

View Article Online
DOI: 10.1039/D5NA00951K

A Supported palladium Schiff-base complex on SBA-15 as reusable supported catalyst in the Heck coupling reaction

Amin Darabi | Mohsen Nikoorazm* | Bahman Tahmasbi*

[1]*Department of Chemistry, Faculty of Science, Ilam University, P. O. Box 69315516, Ilam, Iran.*

[*]*E-mail: m.nikorazm@ilam.ac.ir, b.tahmasbi@ilam.ac.ir*

Abstract

In this study, the mesoporous structure of SBA-15 was synthesized using a very simple procedure, and its surface was modified with 3-aminopropyltriethoxysilane (APTES). Next, (3,4-bis(-(2-hydroxybenzylidene)amino)phenyl)(phenyl)methanone (bis(HBAPPM)) was obtained by condensation of salicylaldehyde (SA) and 1,2-diaminobenzophenone (diABP) in methanol (MeOH), then bis(HBAPPM) was immobilized on the modified mesoporous structure of SBA-15. Then, a palladium Schiff-base complex was supported on the functionalized SBA-15, and the final product was denoted as SBA-15@bis(HBAPPM)-Pd catalyst. The synthesized catalyst was characterized by EDX, XRD, SEM, WDX, TGA, ICP, FT-IR, and BET techniques. The catalytic application of SBA-15@bis(HBAPPM)-Pd was investigated as a heterogeneous catalyst in Heck C – C coupling reaction using various aryl halides and olefins. The result was the achievement of the desired products with excellent yields. Also, the recyclability of the SBA-15@bis(HBAPPM)-Pd nanocatalyst was studied, which showed that this catalyst can be easily isolated from the reaction medium and reused for several consecutive times, which will help us in promoting green chemistry. The recovered SBA-15@bis(HBAPPM)-Pd after reusing from the reaction was characterized by EDX, XRD, SEM, WDX, ICP, and FT-IR techniques.

Keywords: Mesoporous SBA-15, nanocatalyst, palladium, Schiff-base complex, Mizoroki-Heck reaction.

View Article Online
DOI: 10.1039/D5NA00951K

1. Introduction

C – C bond formation is a great and attractive class of organic coupling reactions. These reactions, which are among the most widespread synthetic transformations, have opened a new window to science and played a prominent role in various fields of science such as medicine, chemistry, biochemistry, and nanotechnology [1-3]. Some of the best-known C–C bond formation in organic chemistry include the Heck, Suzuki, Stille, Sonogashira, Kumada, Hiyama, Negishi reactions, etc. [4-11]. Of all the cross-coupling reactions, the Heck reaction is the most important. It was first reported by Richard Heck, hence the name [12]. Heck first reported the coupling of aryl halides (Ar-X) with ethylene in the presence of aryl mercury halides, which was a non-catalytic reaction, in 1968 [2]. Internal alkenes are important intermediates in the pharmaceutical, chemical, polymer and agricultural industries, which Mizoroki-Heck cross-coupling reactions are atom-economic routes to obtain these alkenes [13]. Today, palladium-catalyzed Mizoroki-Heck cross-coupling reactions are an essential part of the synthesis of internal alkene derivatives and are becoming ever more complex and extensive [14]. Nevertheless, some of the reported catalysts face the problem of difficult separation, low recyclability, and high cost of ligands [15-18]. Traditionally, the C-C bond formation is reported in organic solvents at high temperatures using homogeneous or heterogeneous Pd-catalysts, including organic ligands such as phosphines, dibenzylideneacetones and sulfonates [19]. However, organic solvents may cause serious environmental problems and high temperatures definitely consume more cost and energy. Also, most of the phosphine ligands are expensive and sensitive to air and moisture [20, 21]. Moreover, the reuse and isolation of homogeneous catalysts are difficult and environmentally unfriendly [21]. Therefore, the supported catalysts were introduced to combine the advantages of both homogeneous and heterogeneous catalysis, such as high catalytic activity, low amount of metal loaded, easily recyclable, air- and

View Article Online
DOI: 10.1039/D5NA00951K

moisture-stable catalysts as a great importance field in catalyst science [22-26]. Various supports overcome most of these problems by preventing aggregation and providing an active palladium catalytic site [15]. There are various types of supports for the design and synthesis of heterogeneous catalysts with palladium immobilization on them. Some of the supports include mesoporous silica materials [27-29], magnetic nanoparticles [30], boehmite nanoparticles [31], biochar nanoparticles [32], carbon nanotubes [33], graphene oxide [34], zeolites [35], and metal-organic frameworks [36]. Mesoporous silica materials are among the latest achievements in nanotechnology. Due to their amazing chemical and physical properties, such as surface chemistry and pore architecture, these materials have many applications in various fields e.g. catalysis, drug delivery, thermal energy storage, product separation, and biosensors [37-39]. The International Union of Pure and Applied Chemistry (IUPAC) classifies porous materials into 3 categories in terms of the diameter of their pores: microporous materials (less than 2 nm), mesoporous materials (2 to 50 nm), and macroporous materials (greater than 50 nm) [40]. In recent decades, various types of mesoporous structures of Si-materials have been synthesized by modifying the synthesis route and using different surfactants [41]. The most common types of mesoporous silica include MCM (Mobil Composition of Matter), KIT (Korean Advanced Institute of Science and Technology), SBA (Santa Barbara), MSU (Michigan State University), and FDU (Fudan University) [41, 42]. Among a wide range of silica-based structures, mesoporous SBA-15 has been widely investigated as catalyst supports due to its very interesting textural properties such as large and tunable pore diameters, thick walls, high surface area, large pore volume, dual pore architecture, low toxicity, dense silanol (Si-OH) groups on the surface, and excellent chemical stability and also versatile functionalization chemistry [43-45]. Nanocatalysts, which are prepared by immobilizing homogeneous catalysts on solid supports, have both high efficiency and

View Article Online
DOI: 10.1039/D5NA00951K

selectivity, like homogeneous catalysts [46]. Besides, the heterogeneous and insoluble nature of nano-catalysts makes them reusable, like heterogeneous catalysts [47, 48]. Therefore, nanocatalysts do not have the limitations and disadvantages of either homogeneous or heterogeneous catalyst systems [11]. For this reason, nanocatalysts can be called a bridge between homogeneous and heterogeneous catalysts [49]. Therefore, in order to develop new and green methods, here we report a Schiff-base complex of palladium immobilized on mesoporous silica SBA-15 as a novel hybrid nanocatalyst. The catalytic application of this nanocatalyst was investigated and studied in the Mizoroki-Heck carbon-carbon coupling reaction.

2. Experimental

2. 1. Synthesis of bis(HBAPPM) Schiff-base ligand

The (Bis(HBAPPM)) ligand was synthesized via a condensation reaction between SA and diABP (Scheme 1). To synthesize this Schiff-base ligand, first 4 mmol of SA was dissolved in MeOH, then 2 mmol of diABP (in MeOH) was slowly added dropwise to the solution. The reaction lasted for 6 hours at r.t. (room temperature). At the end of the reaction, an orange powder was obtained by evaporating the methanol solvent. The obtained solid product was washed with n-hexane and dried at r.t. [50].

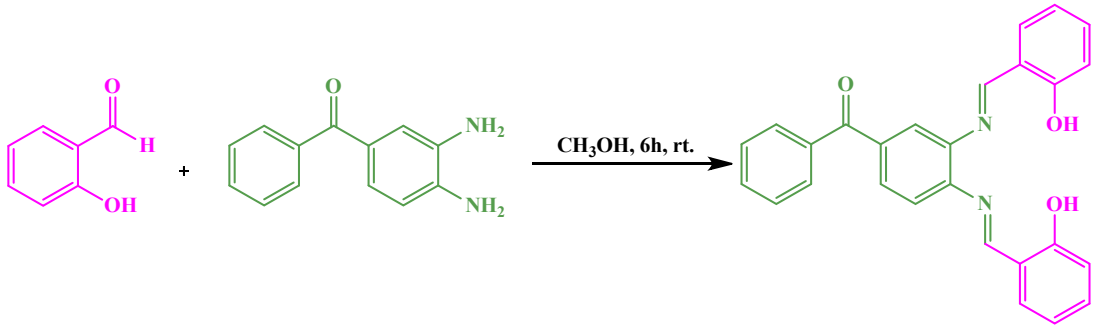

Scheme 1. Synthesis of (3,4-bis(-(2-hydroxybenzylidene)amino)phenyl)(phenyl)methanone Schiff-base ligand (Bis(HBAPPM))

View Article Online
DOI: 10.1039/D5NA00951K

2. 2. Typical procedure for the preparation of mesoporous SBA-15

In the synthesis of the mesoporous structure of SBA-15, the nonionic and polymeric surfactant poly(ethylene glycol) – block - poly(propylene glycol) – block - poly(ethylene glycol) or P123 was used. For this purpose, first, in a 250 mL round-bottom flask, 5.34 g of surfactant P123 was added to a solution of 100 mL of HCl (0.3 M) at room temperature and completely dissolved under magnetic rotation for 12 h. Then, 8.29 g of tetraethyl orthosilicate (TEOS) was slowly injected dropwise into the reaction solution. The reaction was subjected to vigorous mixing at 35 ºC for 24 h. After the desired time, the obtained solution was moved to a Teflon bottle and heated at 100 ºC for 48 h. After that, the cooled mixture was separated using filter paper. The resulting white compound was dried at 100 ºC for 24 h. The resulting white solid powder was extracted with an acidic ethanol solution (a mixture of 1.5 mL of hydrochloric acid and 80 mL of ethanol) for 24 h at 80 ºC. To remove the surfactant pattern, the white powder was calcined at 550 ºC for 5 h at a heating rate of 2 °C/min [51].

2. 3. Modification of SBA-15 with 3-aminopropyltriethoxysilane group

To modify the mesoporous structure of SBA-15, first, 1 g of SBA-15 was dissolved in 30 mL of n-hexane, then 1.5 mL of 3-aminopropyltriethoxysilane was injected into it, and the resulting mixture was heated at 60 ºC for 24 h under reflux and nitrogen atmosphere. The obtained product (SBA-15@APTES) was filtered after cooling to room temperature and washed several times with n-hexane, and the obtained solid was dried at r.t.

View Article Online
DOI: 10.1039/D5NA00951K

2. 4. Functionalization of SBA-15-NPTES with bis(HBAPPM) Schiff-base ligand

First, 1g of the SBA-15@APTES was dispersed in 30 mL of ethanol (EtOH), then 0.86 mmol of bis(HBAPPM) Schiff-base ligand was added to it. The obtained mixture was mixed by a magnetic stirrer under reflux conditions for 24 h at 80 ºC. The obtained product was isolated by simple filtration and washed several times with EtOH. The end, the solid powder (SBA-15@bis(HBAPPM)) was dried at r.t.

2. 5. Immobilization of palladium on SBA-15 toward the preparation of SBA-15@bis(HBAPPM)-Pd nanocatalyst

First, 1 g of functionalized SBA-15 nanoparticles (SBA-15@bis(HBAPPM)) was dispersed in 30 mL of EtOH, then 0.5 mmol of palladium acetate ($Pd(OAc)_2$) was added and mixed by a magnetic stirrer under a nitrogen atmosphere at 80 ºC for 22 h. After the desired time, 0.3 mmol of $NaBH_4$ (sodium borohydride) was added to the reaction mixture and was mixed by a magnetic stirrer under the same conditions for 2 hours. The obtained product (SBA-15@bis(HBAPPM)-Pd) was isolated after cooling, washed with EtOH and water, and finally dried at 50 ºC (Scheme 2).

View Article Online
DOI: 10.1039/D5NA00951K

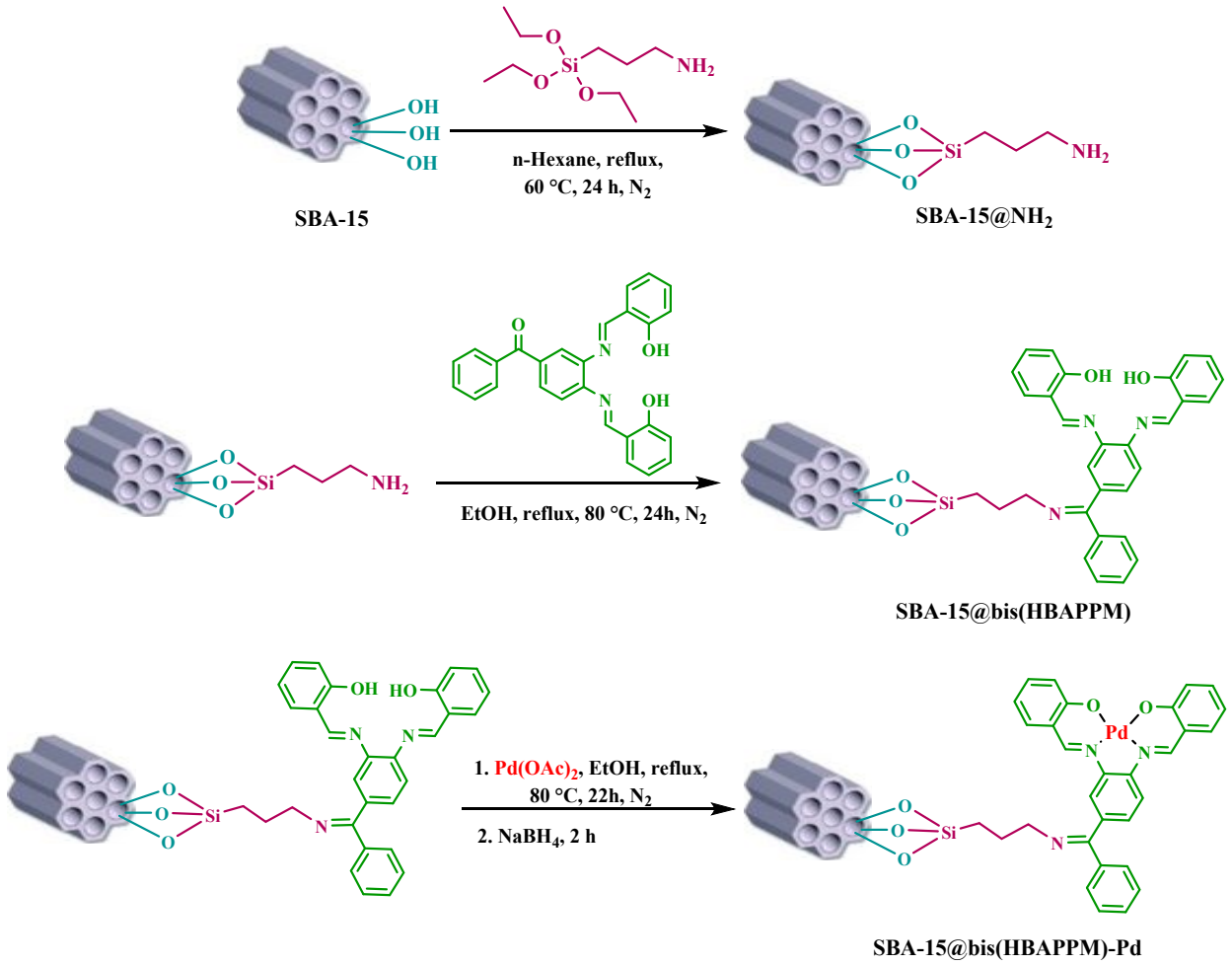

Scheme 2. Synthesis of SBA-15@bis(HBAPPM)-Pd nanocatalyst.

2.6. Typical method for the Mizoroki-Heck C-C cross-coupling reaction catalyzed by SBA-15@ bis(HBAPPM)-Pd nanocatalyst

A mixture of SBA-15@bis(HBAPPM)-Pd nanocatalyst (0.0075 g), butyl acrylate (0.6 mmol), aryl halide (0.5 mmol), base (Na_2CO_3, 1.5 mmol), and 2 mL of PEG-400 (polyethylene glycol 400) as solvent was mixed by a magnetic stirrer at 110 ºC. The progress of the reaction was checked using TLC. After completion of the reaction, the catalyst was removed by a paper filter, and the products were extracted with ethyl acetate. After solvent evaporation, the products with excellent yields were obtained.

View Article Online
DOI: 10.1039/D5NA00951K

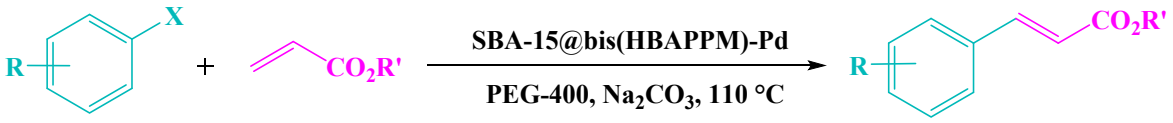

R= H, NO_2, CH_3 **R' = Me, Bu**

X= Br, I

Scheme 3. Heck reaction catalyzed by SBA-15@bis(HBAPPM)-Pd).

2.7. Selected Spectral Data

butyl cinnamate

^{1}H NMR (250 MHz, $CDCl_3$): δ_H= 7.72-7.66 (d, *J*= 15 Hz, 1H), 7.54-7.52 (d, *J*= 5 Hz, 2H), 7.39-7.37 (s, 3H), 6.48-6.42 (d, *J*= 15 Hz, 1H), 4.24-4.19 (t, *J*= 5 Hz, 2H), 1.75-1.64 (quin, *J*= 7.5 Hz, 2H), 1.49-1.37 (sex, *J*= 7.5 Hz, 2H), 1.00-0.94 (t, *J*= 7.5 Hz, 3H) ppm.

butyl cinnamate

^{13}C NMR (100 MHz, $CDCl_3$): δ_C= 167.1, 144.5, 134.5, 130.2, 128.8, 128.0, 118.3, 64.4, 30.8, 19.2, 13.7 ppm.

butyl (E)-3-(4-nitrophenyl)acrylate

^{1}H NMR (250 MHz, $CDCl_3$): δ_H= 8.26-8.23 (d, *J*= 7.5 Hz, 2H), 7.73-7.66 (m, 3H), 6.59-6.53 (d, *J*= 15 Hz, 1H), 4.25-4.20 (t, *J*= 7.5 Hz, 2H), 1.72-1.64 (quin, *J*= 7.5 Hz, 2H), 1.48-1.36 (sex, *J*= 7.5 Hz, 2H), 0.99-0.93 (t, *J*= 7.5 Hz, 3H) ppm.

View Article Online
DOI: 10.1039/D5NA00951K

3. Results and discussion

After the synthesis of the desired catalyst (SBA-15@bis(HBAPPM)-Pd), its structure was fully identified and confirmed using EDX, XRD, SEM, WDX, TGA, FT-IR, and BET techniques.

3. 1. Low-angle XRD pattern

The X-ray diffraction technique was used to obtain more information about the structural characteristics of the SBA-15@bis(HBAPPM)-Pd nanocatalyst. The low angel XRD pattern of the SBA-15@bis(HBAPPM)-Pd nanocatalyst is shown in Figure 1. Similar to SBA-15, the organic-inorganic hybrid material SBA-15@bis(HBAPPM)-Pd also exhibits three distinct diffraction peaks in the range of 2θ = 1.0, 1.50, and 1.80. These peaks correspond to reflections at d_{100}, d_{110}, and d_{200} planes, which are the indices of the highly ordered hexagonal framework of silica [51, 52]. The presence of these peaks indicates that the mesoporous crystalline order of SBA-15 in SBA-15@bis(HBAPPM)-Pd is maintained after loading. While the intensity of the peaks decreased and their angles became smaller, this indicates the decrease in mesoporous order due to the loading of SBA-15 into the pores and the expansion of the unit cell due to the binding of the palladium complex inside the pores, respectively [53].

The normal XRD pattern of the SBA-15@bis(HBAPPM)-Pd nanocatalyst is shown in Figure 2. The normal XRD pattern of the SBA-15@bis(HBAPPM)-Pd nanocatalyst exhibits three distinct diffraction peaks in the range of 2θ ~ 40, 46, and 68. These peaks correspond to reflections at d_{200}, d_{220}, and d_{331} planes, which indice that the chemical state of palladium in the catalyst is Pd(0) [54-56]. The broad peak in the range of 2θ ~ 18-30 is related to amorphous silica [56].

View Article Online
DOI: 10.1039/D5NA00951K

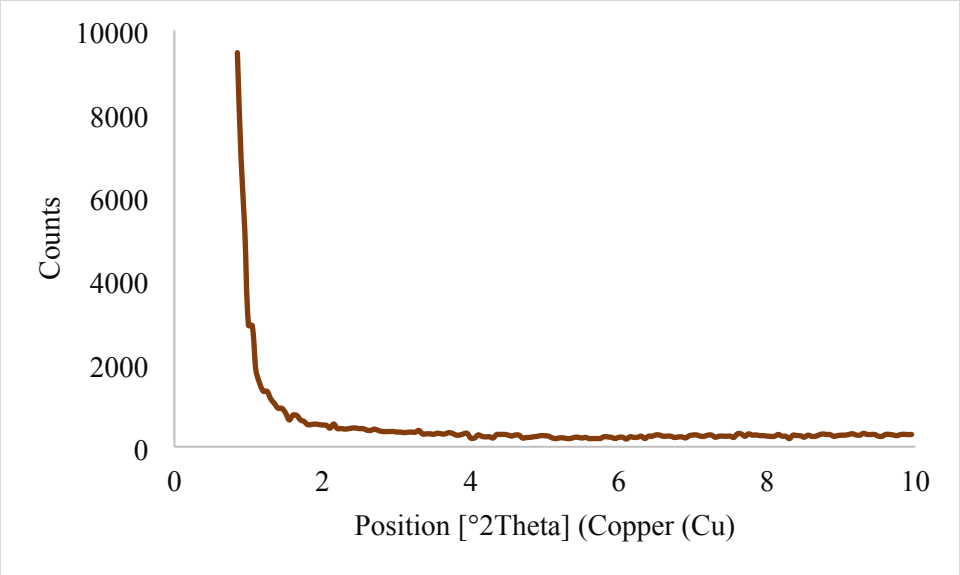

Figure 1. The low-angle XRD pattern of SBA-15@bis(HBAPPM)-Pd nanocatalyst.

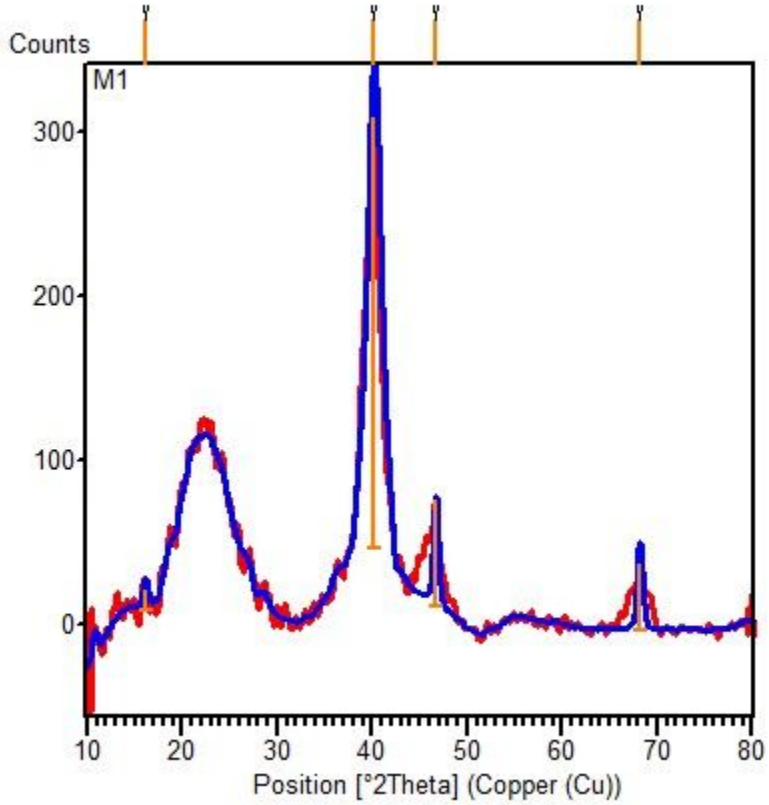

Figure 2. The normal XRD pattern of SBA-15@bis(HBAPPM)-Pd nanocatalyst.

View Article Online
DOI: 10.1039/D5NA00951K

3. 2. BET analysis

Nitrogen adsorption-desorption analysis of the synthesized SBA-15@bis(HBAPPM)-Pd nanocatalyst was carried out under standard temperature and pressure conditions. As shown in Figure 3, this isotherm corresponds to the type IV isotherm and the H_2 hysteresis loop according to the IUPAC classification, which is related to mesoporous materials [57]. The values of the structural and textural parameters related to the catalyst are given in Table 1. The BET analysis data show the surface area (S_{BET}), mean pore diameter (r_p), and total pore volume parameters of the SBA-15@bis(HBAPPM)-Pd nanocatalyst to be 188.89 m^2g^{-1}, 6.231 nm, and 0.294 cm^3g^{-1}, respectively. These data obtained for the catalyst show lower values than those of the mesoporous SBA-15 [58]. This decrease is due to the functionalization process of SBA-15 and the placement of the Schiff-base ligand and palladium atoms within the SBA-15.

Table 1. The surface properties from N_2 adsorption-desorption analysis of SBA-15 and SBA-15@bis(HBAPPM)-Pd nanocatalyst

Sample	S_{BET} (m^2 g^{-1})	r_p (nm)	pore volume (cm^3g^{-1})
SBA-15 [58]	366.0	7.2	0.71
SBA-15@ bis(HBAPPM)-Pd	188.89	6.2319	0.2943

View Article Online
DOI: 10.1039/D5NA00951K

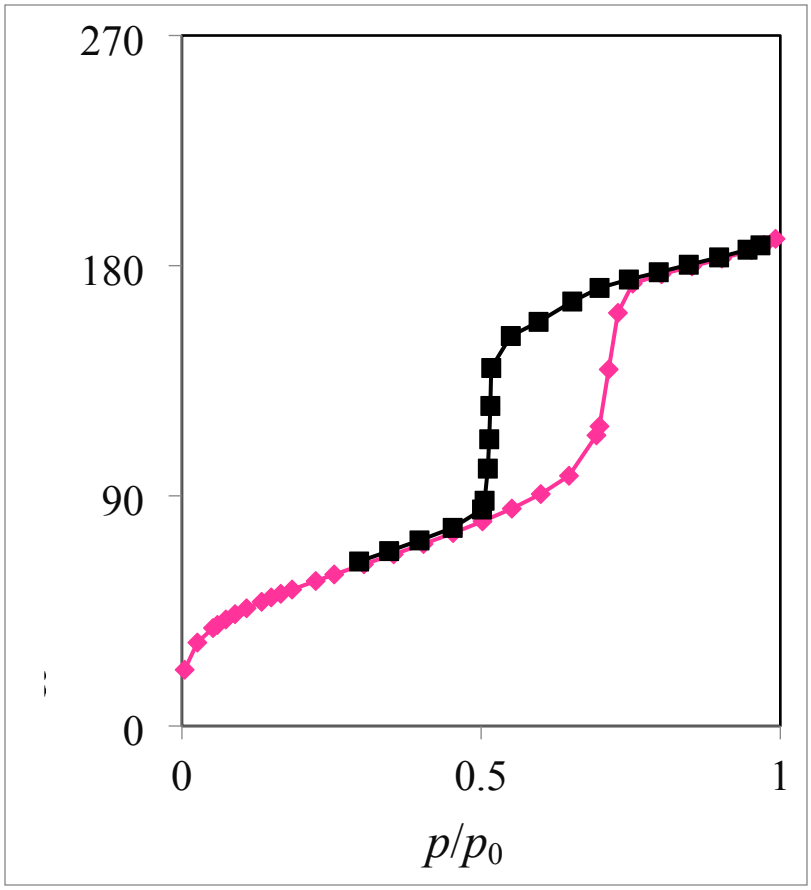

Figure 3. N_2 adsorption–desorption isotherm of SBA-15@bis(HBAPPM)-Pd nanocatalyst.

3. 3. SEM photographs

Figure 4 shows the surface of SBA-15@bis(HBAPPM)-Pd nanocatalyst at high magnification using scanning electron microscopy (SEM). These images show that the morphology of the synthesized catalyst has a uniform particle size distribution. It also confirms the cylindrical shape of the SBA-15 mesoporous material after immobilization of the palladium complex.

View Article Online
DOI: 10.1039/D5NA00951K

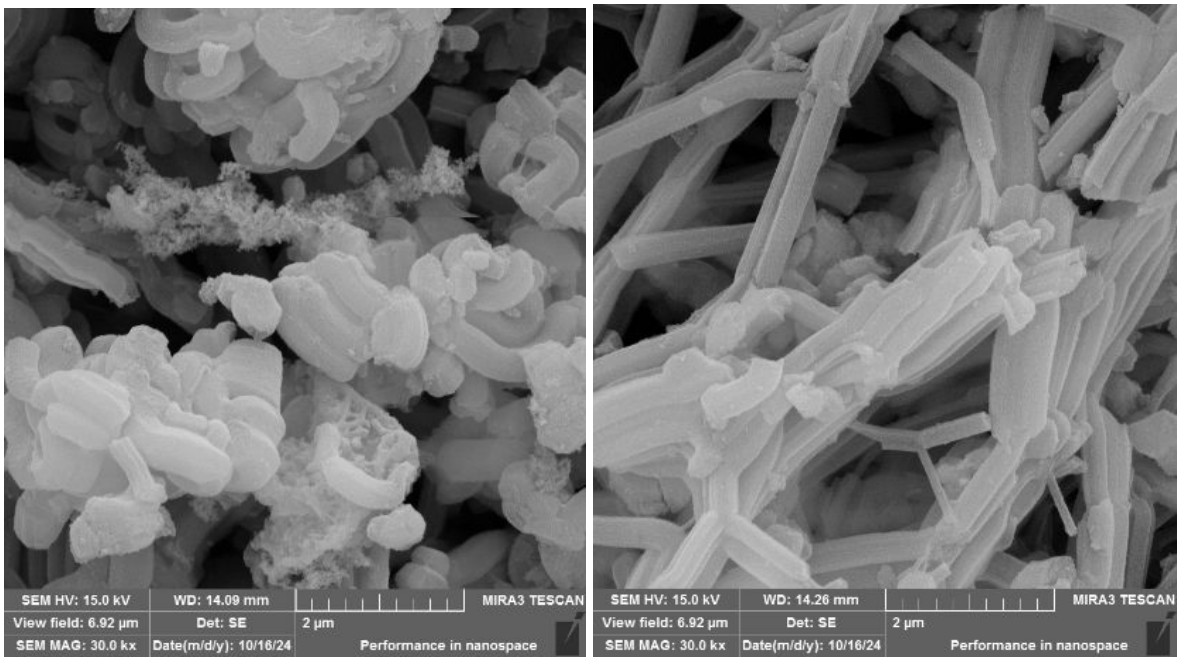

Figure 4. SEM images of SBA-15@bis(HBAPPM)-Pd nanocatalyst.

3. 4. Energy-dispersive X-ray analysis, elemental-mapping and inductively coupled plasma

The energy dispersive X-ray (EDX) spectrum of the SBA-15@bis(HBAPPM)-Pd nanocatalyst for determining the elemental composition is shown in Figure 5. The EDX pattern confirms the peaks corresponding to the Si, O, C, N, and Pd species in the structure of this catalyst. Also, to determine the distribution of elements, WDX analysis was used, the images of which are shown in Figure 6. As can be seen in the elemental mapping images, the elements Si, O, C, N, and Pd are uniformly dispersed in the structure of the SBA-15@bis(HBAPPM)-Pd nanocatalyst.

Also, the amount of palladium in SBA-15@bis(HBAPPM)-Pd catalyst was investigated using ICP analysis. The exact amount of palladium in SBA-15@bis(HBAPPM)-Pd catalyst was obtained as 1.4×10^{-3} mol.g^{-1}.

View Article Online
DOI: 10.1039/D5NA00951K

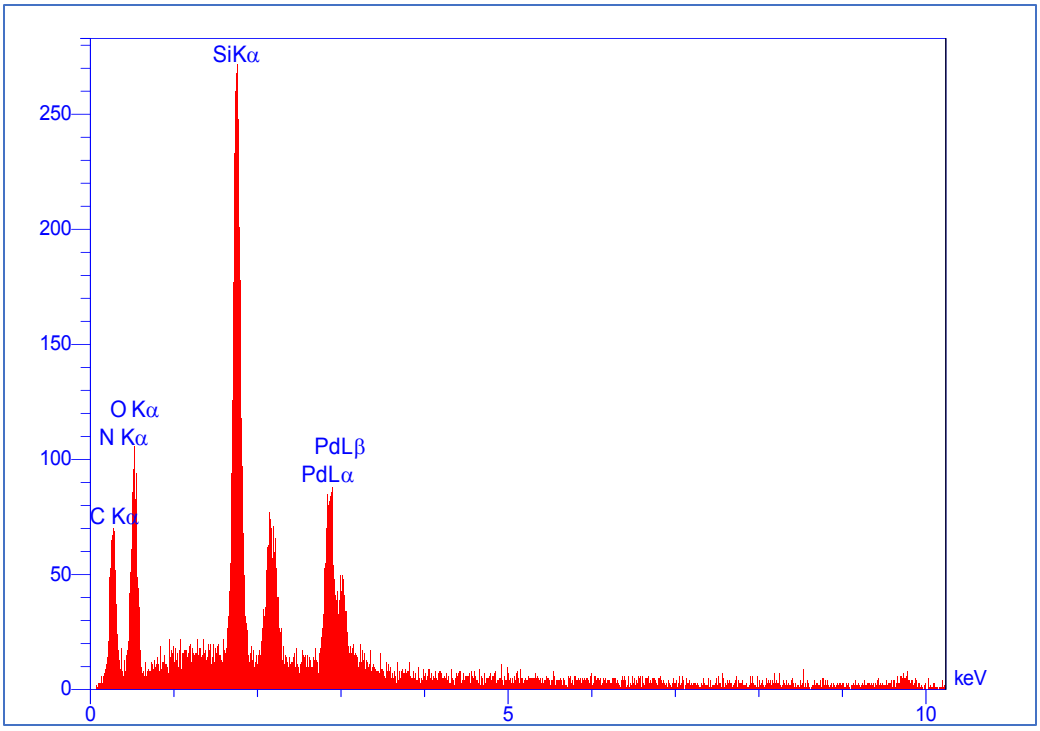

Figure 5. The EDX analysis of SBA-15@bis(HBAPPM)-Pd nanocatalyst.

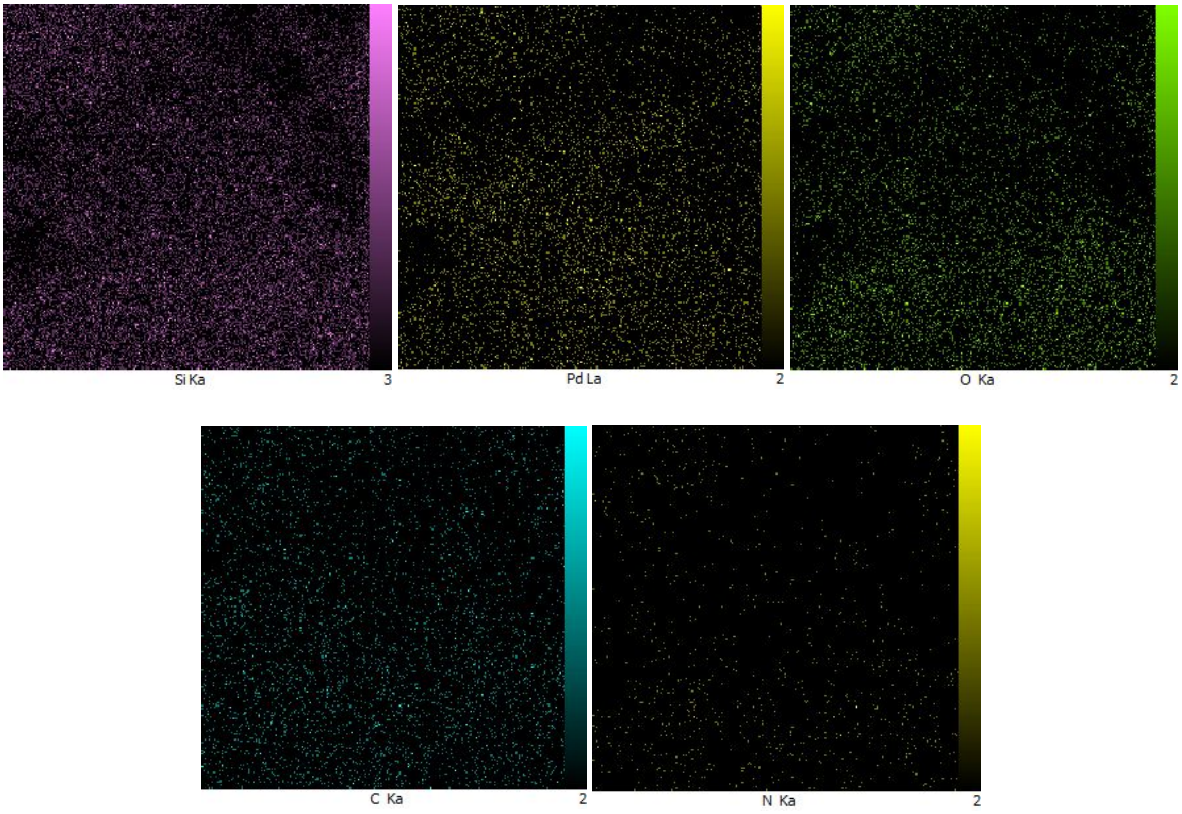

Figure 6. WDX elemental mapping images of SBA-15@bis (HBAPPM)-Pd nanocatalyst.

View Article Online
DOI: 10.1039/D5NA00951K

3. 5. TGA analysis

TGA analysis was used to demonstrate the immobilization of organic groups on the SBA-15 support. The TGA curve for SBA-15@bis (HBAPPM)-Pd is shown in Figure 7. The weight loss below 100°C is related to the evaporation of adsorbed solvents. The weight loss of 19.34% in the temperature range of 200–500 °C is related to the thermal decomposition of organic species immobilized on the mesoporous SBA-15 [59].

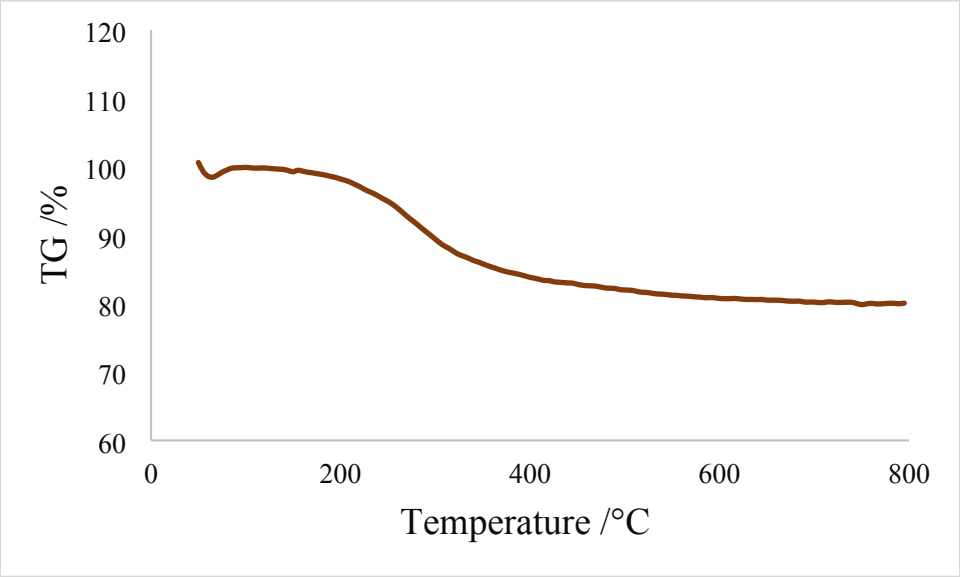

Figure 7. TGA curve of SBA-15@bis (HBAPPM)-Pd nanocatalyst.

3. 6. FT-IR spectra

Figure 8 illustrates the IR spectra of the synthesis steps of the nanocatalyst, including (a) SBA-15, (b) modified SBA-15@APTES, (c) SBA-15@bis(HBAPPM), (d) SBA-15@bis(HBAPPM)-Pd, and (e) bis(HBAPPM) ligand. In spectrum (a), the prominent peak at 3433 cm^{-1} is attributed to the O-H stretching vibration on the SBA-15 surface. The sharp peak at 1080 cm^{-1} is related to the asymmetric stretching vibration of the Si-O- Si, and the clear peak at 804 cm^{-1} is related to the symmetric stretching vibration of the Si-O, and the peak at 461 cm^{-1} is related to the Si-O-Si bending vibration frequency [60, 61]. In spectrum (b), which is related to the SBA-15@APTES

View Article Online
DOI: 10.1039/D5NA00951K

material, the peaks related to the NH_2 bending vibration appeared at 1492 cm^{-1} and 1567 cm^{-1}, and the stretching vibration from the NH_2 group at 3439 cm^{-1}. Also, the peak related to the C-H stretching vibration was observed at 2934 cm^{-1} [62]. The presence of these peaks indicates that the modification of the SBA-15 support surface was successful. In the spectrum of SBA-15@bis(HBAPPM), a distinct peak was displayed in the 1636 cm^{-1} region, which is referred to as the stretching vibration of the imine bond C=N [50, 63]. In the FT-IR spectrum of SBA-15@bis(HBAPPM)-Pd, the presence of the bands 461, 799, and 1077 cm^{-1} confirms that the structure of SBA-15 remains unchanged after surface modification and palladium complex immobilization.

View Article Online
DOI: 10.1039/D5NA00951K

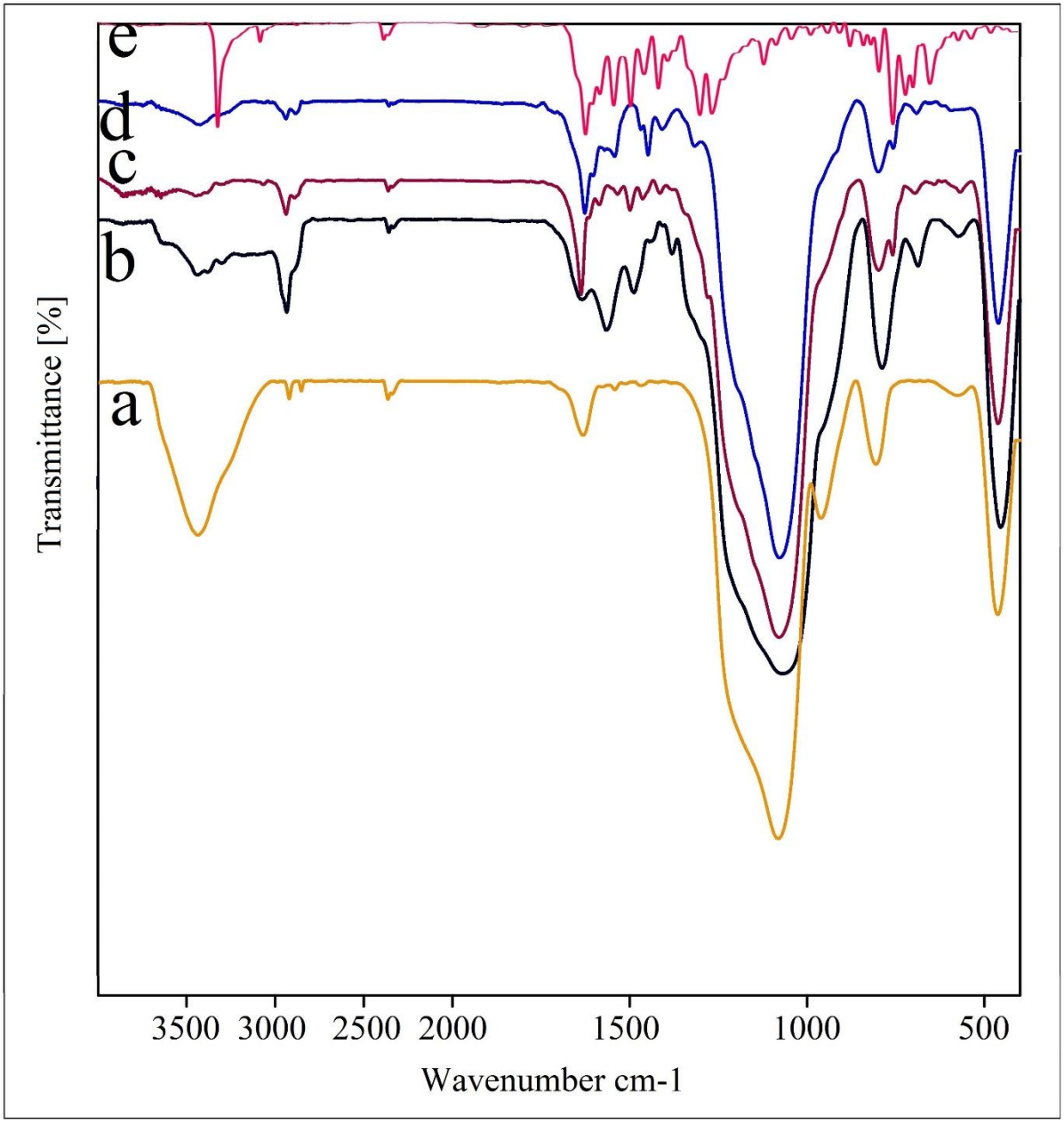

Figure 8. FT-IR spectra of (a) SBA-15, (b) modified SBA-15@NPTES, (c) SBA-15@ bis(HBAPPM), (d) SBA-15@bis(HBAPPM)-Pd nanocatalyst, and (e) bis(HBAPPM) ligand.

3. 7. Catalytic Studies

To investigate the catalytic performance of SBA-15@bis(HBAPPM)-Pd in the Heck carbon-carbon coupling reaction, the reaction between butyl acrylate and iodobenzene (PhI) was selected

View Article Online
DOI: 10.1039/D5NA00951K

as a model coupling reaction in the first step. At first, the model coupling reaction was examined in the presence of SBA-15 and SBA-15@bis(HBAPPM) as a catalyst (Table 2, entries 1 and 2), where no product was obtained even after 300 minutes. Therefore, the presence of palladium is essential for the Heck coupling reaction.

Table 2. A comparison of SBA-15@bis(HBAPPM)-Pd with SBA-15 or SBA-15@bis(HBAPPM) as catalyst (Catalyst (15 mg), butyl acrylate (1.2 mmol), iodobenzene (1 mmol), Na_2CO_3 (3 mmol), and PEG-400 solvent, at 110 °C).

Entry	Catalyst	Time (min)	Yield (%)
1	SBA-15	300	-
2	SBA-15@bis(HBAPPM)	300	-
3	SBA-15@bis(HBAPPM)-Pd	30	97

In the following, different reaction conditions such as the effective amount of catalyst, the effect of solvent, the effect of temperature, and the effect of the type and amount of base were tested. The results of these experiments are given in Table 2. Initially, the effect of the catalyst condensation on the sample reaction was studied in the presence of different amounts including no catalyst, 10, 12, 15, and 20 mg (Table 2, entries 1-5). The best and ideal result was achieved with an amount of 15 mg of catalyst. Reducing or increasing this amount of catalyst did not significantly improve the reaction yield. According to the results obtained, an amount of 15 mg of nanocatalyst was considered the optimal amount. In the next step, the effect of the solvent was evaluated. Different types of solvents, such as PEG-400, EtOH, DMF, toluene, DMSO, and H_2O were tested and investigated, and the best and ideal results were obtained in the PEG-400 solvent (Table 2, entry 4). After investigating the effect of the solvent, the effect of different bases was checked, and

View Article Online
DOI: 10.1039/D5NA00951K

among the bases Na_2CO_3, NaOH, $N(CH_2CH_3)_3$, K_2CO_3, and NaOEt, the Na_2CO_3 base was selected as the most effective base. Finally, the effect of temperature was tested at temperatures of 60, 90, and 110 °C. It was found that the reaction at a temperature of 110 °C has the best efficiency (Table 2, entries 4, 15, 16).

In summary, the results in the table show that the conditions selected for carrying out the Heck reaction are the use of Ar-X (1 mmol) with butylacrylate (1.2 mmol) in the presence of 15mg of SBA-15@bis(HBAPPM)-Pd catalyst, 3 mmol of Na_2CO_3 base, in PEG-400 solvent and at a temperature of 110 °C (Table 2, entry 4).

Table 2. Experimental optimization of the Heck reaction of n-butyl acrylate and iodobenzene in the presence of SBA-15@bis(HBAPPM)-Pd nanocatalyst[a].

Entry	Solvent	Base	Base (mmol)	Catalyst (mg)	Temperature (°C)	Time (min)	Yield (%)[b]
1	PEG-400	Na_2CO_3	3	-	110	300	-
2	PEG-400	Na_2CO_3	3	10	110	75	89
3	PEG-400	Na_2CO_3	3	12	110	60	90.5
4	PEG-400	Na_2CO_3	3	15	110	30	97
5	PEG-400	Na_2CO_3	3	20	110	30	97
6	EtOH	Na_2CO_3	3	15	80	195	87
7	H_2O	Na_2CO_3	3	15	100	420	87
8	DMF	Na_2CO_3	3	15	110	90	91
9	DMSO	Na_2CO_3	3	15	110	180	-
10	Toluene	Na_2CO_3	3	15	110	180	-
11	PEG-400	NaOEt	3	15	110	90	88
12	PEG-400	NaOH	3	15	110	210	90
13	PEG-400	$N(CH_2CH_3)_3$	3	15	110	120	89
14	PEG-400	K_2CO_3	3	15	110	120	92
15	PEG-400	Na_2CO_3	3	15	90	90	89
16	PEG-400	Na_2CO_3	3	15	60	240	80
17	PEG-400	Na_2CO_3	2	15	110	80	91
18	PEG-400	Na_2CO_3	1	15	110	120	90

[a]Reaction conditions: SBA-15@bis(HBAPPM)-Pd nanocatalyst (0-20 mg), butyl acrylate (1.2 mmol), iodobenzene (1 mmol), base (1-3 mmol), and solvent (2 mL), at 60-110 °C.
[b]Isolated yield.

View Article Online
DOI: 10.1039/D5NA00951K

The catalytic application of SBA-15@bis(HBAPPM)-Pd in the synthesis of a wide range of methyl cinnamate or butyl cinnamate derivatives was tested on a number of different aryl halides under the optimized conditions, which are summarized in Table 3. The results of these experiments are summarized in Table 3, which shows that the desired methyl cinnamate or butyl cinnamates were synthesized in good yields. TOF and TON values indicate that aryl halides with electron-withdrawing groups are more reactive than aryl halides with electron-donating groups in the Heck carbon-carbon coupling reaction in the presence of an SBA-15@bis(HBAPPM)-Pd catalyst.

Table 3. Heck reaction in the presence of SBA-15@bis(HBAPPM)-Pd nanocatalyst[a].

Entry	X	R	R'	Time (min)	Yield[b] (%)	TON	TOF (h^{-1})
1	I	H	Bu	30	97	46.19	92.38
2	Br	H	Bu	40	94	44.76	67.14
3	Br	4-NO_2	Bu	30	96	45.71	91.43
4	I	4-NO_2	Bu	30	94	44.76	89.52
5	I	H	Me	60	95	45.24	45.24
6	Br	H	Me	85	95	45.24	31.93
7	I	4-CH_3	Me	65	94	44.76	41.32
8	Br	4-NO_2	Me	95	93	44.28	27.97
9	Br	4-CH_3	Me	95	95	45.24	28.57
10	I	4-NO_2	Me	50	94	44.76	53.71

[a]Reaction conditions: SBA-15@bis(HBAPPM)-Pd nanocatalyst (15 mg), methyl acrylate or butyl acrylate (1.2 mmol), aryl halide (1 mmol), Na_2CO_3 (3 mmol), and PEG-400 solvent, at 110 °C.
[b]Isolated yield.

The proposed catalytic mechanism for the Heck carbon-carbon coupling reaction catalyzed by SBA-15@bis(HBAPPM)-Pd is presented in Scheme 4. The cycle consists of an (1) oxidative addition, (2) an insertion step, (3) a beta-hydride elimination step, and (4) a reductive elimination step, which at the end of the catalyst is recycled and returned to the cycle [54, 64-68]. In the

View Article Online
DOI: 10.1039/D5NA00951K

oxidative addition step, the Pd(0) is converted to Pd(II) after the addition of the aryl halide. In the Insertion step, an olefinic species is added, and a new C-C bond is formed. In the β-hydride elimination step, the H-atom is migrated, and palladium hydride and products are formed. Finally, in the reductive elimination step, the Pd(0) is regenerated by a reduction reaction [69].

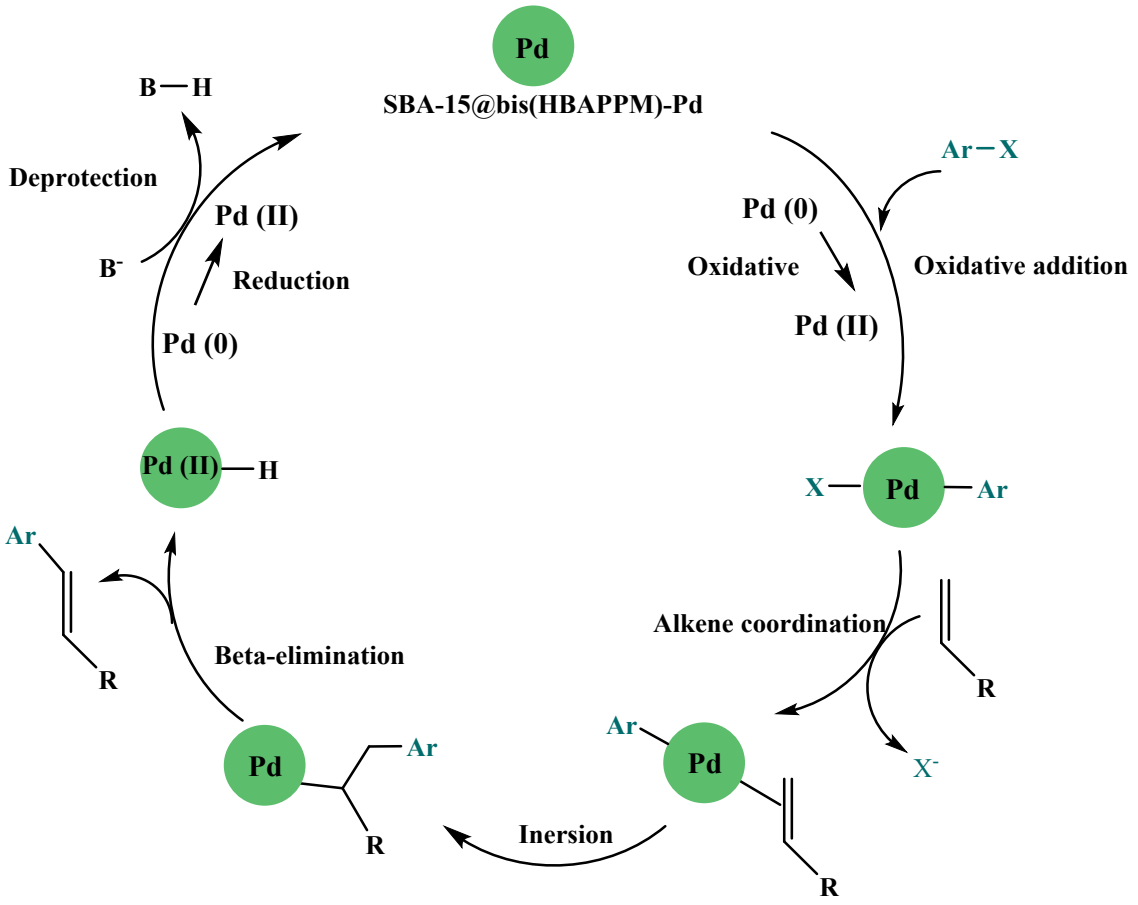

Scheme 4. Proposed mechanism for the Heck carbon-carbon coupling reaction in the presence of SBA-15@bis(HBAPPM)-Pd nanocatalyst.

3. 8. Reusability of SBA-15@bis (HBAPPM)-Pd catalyst

Recyclability is the most important feature of catalytic systems. The SBA-15@bis(HBAPPM)-Pd catalyst is a heterogeneous catalyst that is easily separated from the product after reaction by

View Article Online
DOI: 10.1039/D5NA00951K

simple filtration. Hence, it can be easily used to carry out the reaction again. This is a proof of the value and greenness of a catalyst. Therefore, the reaction between PhI and butyl acrylate under the optimal conditions in Table 2 was considered as a model reaction to start recycling. After reaction, SBA-15@bis(HBAPPM)-Pd catalyst was isolated from the reaction mixture by filter paper and thoroughly washed using ethyl acetate solvent. After drying at 50 °C, it was used for reuse under the same conditions. As shown in Figure 9, the recycling of SBA-15@bis(HBAPPM)-Pd catalyst is repeated several times. This catalyst, with almost constant catalytic activity, can be recycled up to 5 times. The excellent reusability may result from the strong bond between the palladium complex and the SBA-15 support, which effectively prevents palladium leaching.

The stability and heterogeneous nature of SBA-15@bis(HBAPPM)-Pd were investigated by a hot filtration test based on a published article [70]. In this regard, in the synthesis of butyl cinnamate from the coupling of iodobenzene with butyl acrylate, the catalyst was removed after 15 min, and the remaining mixture was allowed to react for 30 min without the catalyst. In this hot filtration test, the butyl cinnamate product was obtained with a 67% yield. These results indicate that no significant leaching of palladium occurred during the reaction. Also, the coupling reaction of iodobenzene with butyl acrylate was repeated, and after 30 minutes, the SBA-15@bis(HBAPPM)-Pd catalyst was isolated by simple filtration. The amount of palladium in the filtered solution and the recovered SBA-15@bis(HBAPPM)-Pd catalyst was checked using ICP analysis. No leached palladium was observed in the filtered solution. Also, the exact amount of palladium in the recovered SBA-15@bis(HBAPPM)-Pd catalyst was obtained as 1.2×10^{-3} mol.g^{-1}, which does not change significantly compared to the palladium present in the fresh catalyst (1.4×10^{-3} mol.g^{-1}). Therefore, it can be said with certainty that palladium leaching from the catalyst did not occur under the Heck C-C coupling reaction conditions.

View Article Online
DOI: 10.1039/D5NA00951K

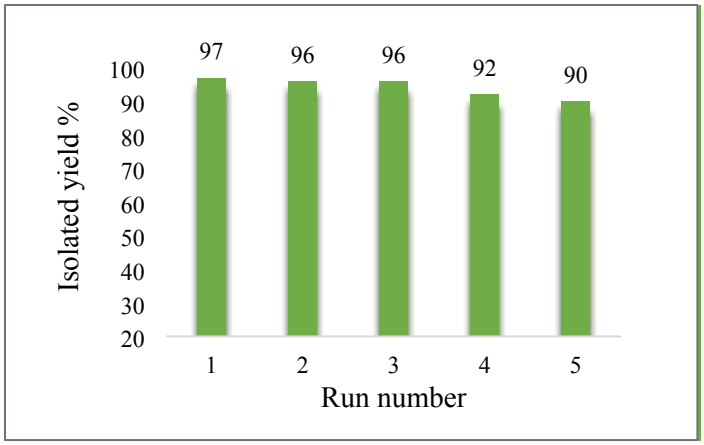

Figure 9. The reusability of SBA-15@bis(HBAPPM)-Pd nanocatalyst in the model reaction of butyl cinnamate synthesis.

3. 9. The post-recovery characterization of SBA-15@bis(HBAPPM)-Pd catalyst

The post-recovered SBA-15@bis(HBAPPM)-Pd nanocatalyst was characterized by EDX, XRD, SEM, WDX, ICP, and FT-IR techniques, and was matched with a fresh catalyst.

The low-angel XRD pattern of the post-recovered SBA-15@bis(HBAPPM)-Pd nanocatalyst is shown in Figure 10. Similar to fresh SBA-15@bis(HBAPPM)-Pd, the low-angel XRD pattern of the post-recovered catalyst shows three distinct 2θ diffraction peaks, which are indicators of the stability of this catalyst.

View Article Online
DOI: 10.1039/D5NA00951K

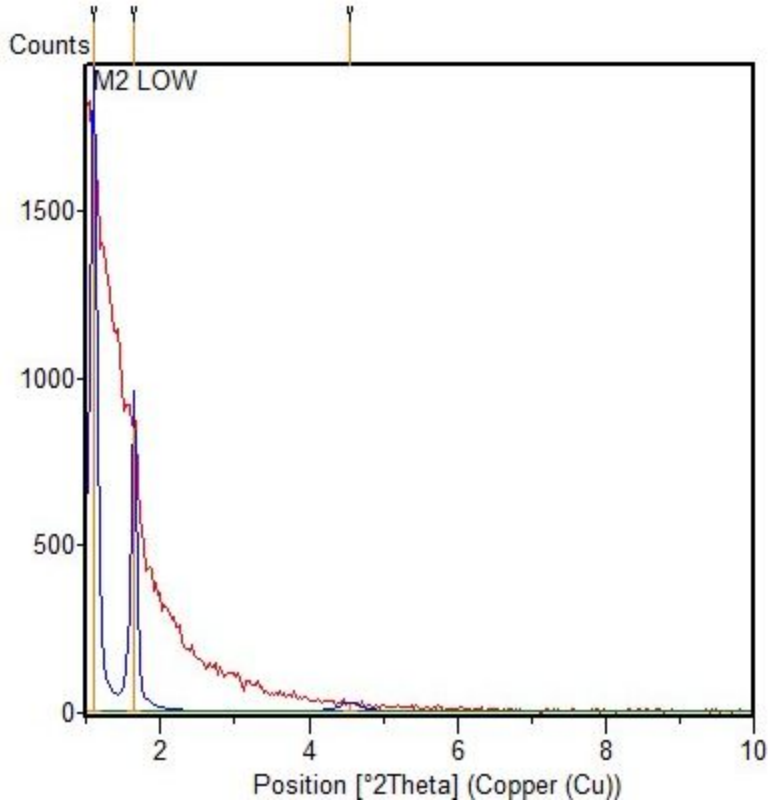

Figure 10. The low-angle XRD pattern of the post-recovered SBA-15@bis(HBAPPM)-Pd nanocatalyst.

Figure 11 illustrates the IR spectra of the fresh SBA-15@bis(HBAPPM)-Pd and post-recovered SBA-15@bis(HBAPPM)-Pd. The IR spectrum of the post-recovered catalyst is in perfect agreement with the IR spectrum of the fresh catalyst, indicating the stability of the catalyst under the reaction conditions after recovery.

View Article Online
DOI: 10.1039/D5NA00951K

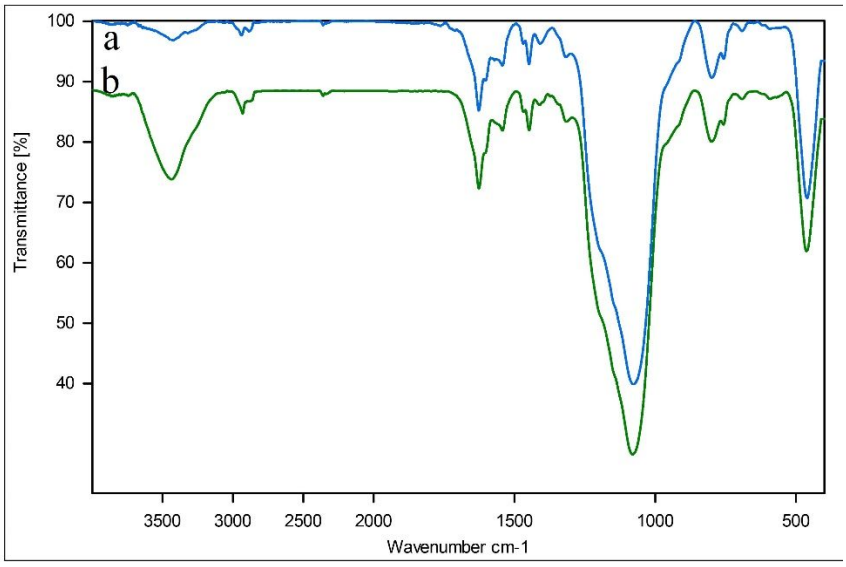

Figure 11. FT-IR spectra of (a) SBA-15@bis(HBAPPM)-Pd nanocatalyst, and (b) the post-recovered SBA-15@bis(HBAPPM)-Pd nanocatalyst.

Figure 12 shows the SEM image of the post-recovered SBA-15@bis(HBAPPM)-Pd nanocatalyst. This image shows that the morphology of the post-recovered catalyst has a uniform particle size distribution, similar to that of the fresh catalyst. The morphology and particle size of the catalyst remained unchanged after recycling, indicating the stability of the catalyst after recycling.

View Article Online
DOI: 10.1039/D5NA00951K

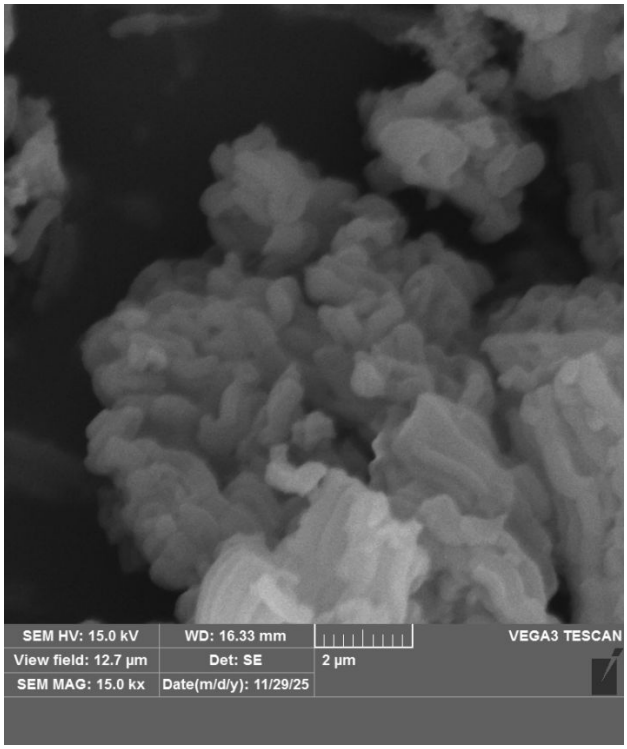

Figure 12. SEM images of the post-recovered SBA-15@bis(HBAPPM)-Pd nanocatalyst.

The EDX spectrum and WDX mapping of the post-recovered SBA-15@bis(HBAPPM)-Pd catalyst are shown in Figures 13 and 14. The EDX pattern of the post-recovered catalyst (Figure 13) confirms the presence of the Si, O, C, N, and Pd species, similar to that of the fresh catalyst. Also, WDX analysis of the post-recovered catalyst (Figure 14) shows that all elements are uniformly dispersed in the structure of the recovered nanocatalyst.

Also, the amount of palladium in the post-recovered SBA-15@bis(HBAPPM)-Pd catalyst was calculated as 1.2×10^{-3} mol.g^{-1}, which does not change significantly compared to the palladium present in the fresh catalyst (1.4×10^{-3} mol.g^{-1}). Therefore, palladium leaching from the catalyst did not occur under the Heck C-C coupling reaction conditions.

View Article Online
DOI: 10.1039/D5NA00951K

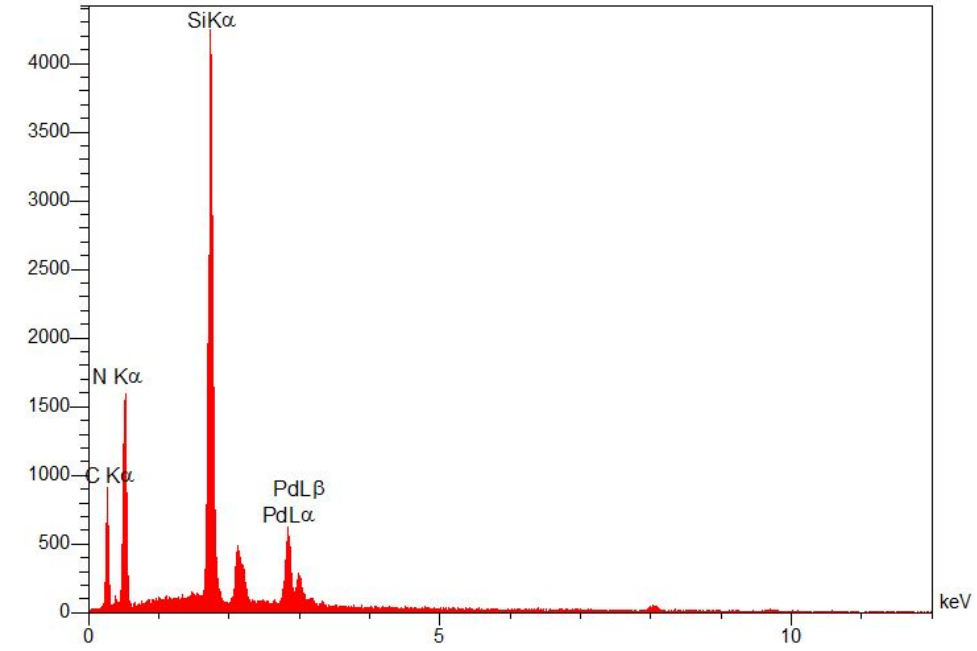

Figure 13. The EDX analysis of the post-recovered SBA-15@bis(HBAPPM)-Pd nanocatalyst.

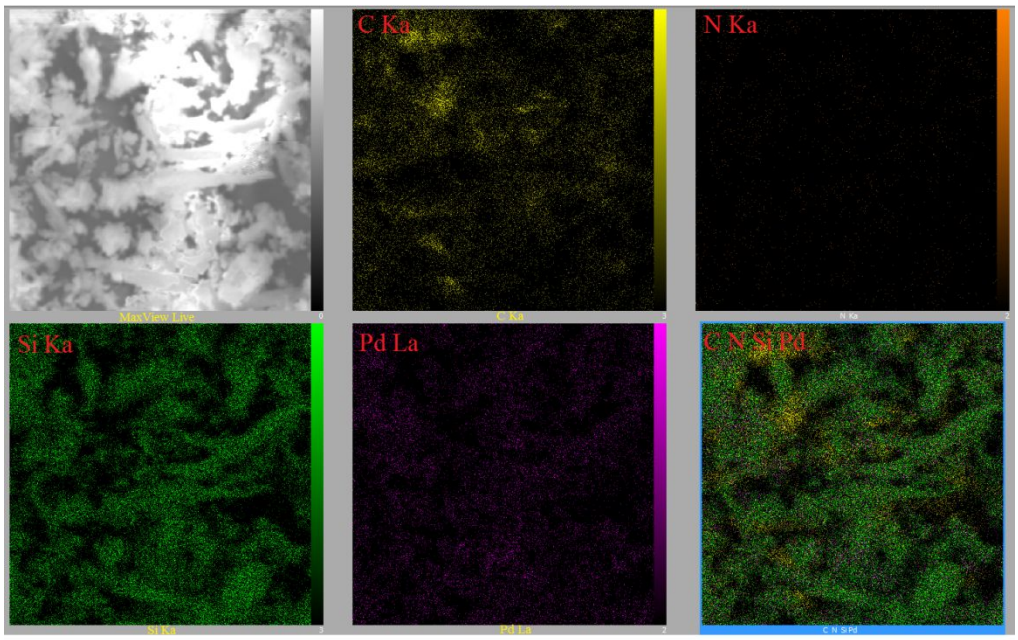

Figure 14. WDX elemental mapping images of the post-recovered SBA-15@bis (HBAPPM)-Pd nanocatalyst.

View Article Online
DOI: 10.1039/D5NA00951K

3. 10. Comparison of the catalyst

Table 4 compares the performance and activity of the SBA-15@bis(HBAPPM)-Pd catalyst with previous catalysts reported for this reaction. The comparison was made for the reaction of PhI with butyl acrylate. As is clear, this reaction was carried out using SBA-15@bis(HBAPPM)-Pd catalyst and in the green solvent PEG-400 in a shorter time with high efficiency. In addition, the SBA-15 support is a cheap and environmentally friendly support. Also, SBA-15@bis(HBAPPM)-Pd is a heterogeneous catalyst and is easily separated from the reaction medium. In some cases, toxic solvents, expensive catalysts, or homogeneous and non-recyclable catalysts have been used, which are difficult to separate from the reaction medium.

Table 4. Comparison of SBA-15@bis(HBAPPM)-Pd nanocatalyst for the Heck reaction with reported catalysts in literature.

Entry	Reported Catalysts	Conditions reaction	Time (min)	Yield (%)	Ref.
1	boehmite@tryptophan-Pd	DMSO, K_2CO_3, 120 °C	85	95	[71]
2	f-CNTs-Pd	DMF, Et_3N,100 °C	7.5 h	64.2	[72]
3	Pd@NHC-MOP	DMF, Et_3N,130 °C	60	99	[73]
4	C-(KTB-Pd)	DMF, $K_3PO_4 \cdot 3H_2O$, , 120 °C	120	99	[74]
5	Pd(II)-SBA-16	H_2O, K_2CO_3, 80 °C	60	97	[75]
6	Pd/SBA-15	DMF, Et3N, 100 °C	12 h	88	[76]
7	Bis(oxamato)palladate(II)	DMF, Et_3N,80 °C	180	94	[77]
8	SBA-15@bis(HBAPPM)-Pd	PEG-400, Na_2CO_3, 110 °C	30	97	Current study

4. Conclusion

SBA-15 nanoparticles are used as a suitable support for stabilizing metal complexes and producing heterogeneous nanocatalysts, which, in addition to increasing catalytic activity, allow for convenient and easy separation of metal complexes. In this study, SBA-15@bis(HBAPPM)-Pd, as a new nanocatalyst, was first synthesized by immobilization of palladium complex in the mesoporous channels of SBA-15, then characterized by EDX, XRD, SEM, WDX, TGA, FT-IR,

View Article Online
DOI: 10.1039/D5NA00951K

and BET techniques. The prepared catalyst was used in the Mizoroki-Heck carbon-carbon coupling reaction, which is known as one of the important reactions in organic chemistry. The carbon-carbon coupling reaction is important in the synthesis of biologically active compounds, organic building blocks, natural synthetic compounds, and pharmaceutical compounds and intermediates. The advantages of this catalytic system include minimal time and cost, no waste generation, production of products with good yields and short reaction times, use of green solvents, simplicity of operation, ease of catalyst recovery, and good performance under reaction conditions. In addition, SBA-15@bis(HBAPPM)-Pd is economically viable and environmentally friendly due to the negligible Pd washout.

Declaration of Interest Statement

- Authors declare no conflict of interest. There was no funding for this work, but experimental work was carried out using the facilities of Ilam University, which are mentioned in the Acknowledgements section.
- The authors consent to the publication of the article.
- Authors declare no conflict of interest.

Clinical trial

"Clinical Trial: Not applicable"

Acknowledgments

Authors thank the research facilities of Ilam University, Ilam, Iran, for financial support of this research project.

Data Availability

"All data generated or analyzed during this study are included in this published article and Supporting Information."

View Article Online
DOI: 10.1039/D5NA00951K

Author Contributions Statement

Amin Darabi: Methodology, Validation, Investigation, Writing-Original Draft,

Bahman Tahmasbi: Conceptualization, Resources, Writing-Original Draft, Project administration

Mohsen Nikoorazm: Formal analysis, Resources, Writing - Review & Editing, Project administration

References

[1] Tamami, B., & Dodeji, F. N. *Journal of the Iranian Chemical Society*. **2012**, *9*, 841-850.

[2] Molnár, Á. *Chemical reviews*. **2011**, *111*(3), 2251-2320.

[3] Nikoorazm, M., Ghorbani, F., Ghorbani-Choghamarani, A., & Erfani, Z. *Applied Organometallic Chemistry*. **2018**, *32*(4), e4282.

[4] Nikoorazm, M., Ghorbani-Choghamarani, A., & Khanmoradi, M. *Applied Organometallic Chemistry*. **2016**, *30*(8), 705-712.

[5] Hegde, S., Nizam, A., & Vijayan, A. *New Journal of Chemistry*. **2024**, *48*(3), 1121-1129.

[6] King, A. K., Brar, A., Li, G., & Findlater, M. *Organometallics*. **2023**, *42*(17), 2353-2358.

[7] Majhi, S., & K. Jash, S. *Synthetic Communications*. **2023**, *53*(24), 2061-2087.

[8] Keskin, S., Çıtlakoğlu, M., Akbayrak, S., & Kaya, S. *Journal of Colloid and Interface Science*. **2022**, *623*, 574-583.

[9] Li, K., Zu, B., & Mazet, C. *Organic Letters*. **2024**, 26(28), 6047-6052.

[10] Gong, H. P., Quan, Z. J., & Wang, X. C. *Journal of Chemical Research*. **2022**, *46*(1), 17475198211067163.

[11] Yangyang, W., Jingping, Q., & Yifeng, C. *Chinese Journal of Organic Chemistry*. **2021**, *41*(5), 1949.

[12] Hagiwara, H.; Sugawara, Y.; Hoshib, T.; Suzuki, T. *Chem. Commun*. **2005**, 2942-2944.

[13] Turan, N., Buldurun, K., Bursal, E., & Mahmoudi, G. *Journal of Organometallic Chemistry*. **2022**, *970*, 122370.

[14] Balanta, A., Godard, C., & Claver, C. *Chemical Society Reviews*. **2011**, *40*(10), 4973-4985

[15] Abdellah, A. R., El-Adasy, A. B. A., Atalla, A. A., Aly, K. I., & Abdelhamid, H. N. *Microporous and Mesoporous Materials*. **2022**, *339*, 111961.

[16] Gaikwad, D. S., Park, Y., & Pore, D. M. *Tetrahedron Letters*. **2012**, *53*(24), 3077-3081.

[17] Ye, J., Chen, W., & Wang, D. *Dalton Transactions*. **2008**, (30), 4015-4022.

[18] Mandegani, Z., Asadi, M., Asadi, Z., Mohajeri, A., Iranpoor, N., & Omidvar, A. *Green Chemistry*. **2015**, *17*(6), 3326-3337.

View Article Online
DOI: 10.1039/D5NA00951K

[19] Hervé, G., Sartori, G., Enderlin, G., Mackenzie, G., & Len, C., *RSC Advances*, **2014**, *4*, 18558-18594.

[20] Zhang, D., & Wang, Q., *Coordination Chemistry Reviews*, **2015**, *286*, 1-16.

[21] Le, X., Dong, Z., Jin, Z., Wang, Q., & Ma, J., *Catalysis Communications*, **2014**, *53*, 47-52.

[22] Emad-Abbas, N., Naji, J., Moradi, P., & Kikhavani, T., *RSC Advances*, **2024**, *14*, 22147–22158

[23] Norouzi, M., & Moradi, P., *Biomass Conversion and Biorefinery*, **2025**, *15*, 2465–2477.

[24] Tahmasbi, B., Moradi, P., Mohammadi, F., Abbasi Tyula, Y., & Kikhavani, T., *Applied Organometallic Chemistry*, **2025**, *39(1),* e7791.

[25] Norouzi, M., Moradi, P., & Khanmoradi, M., *RSC Advances*, **2023**, *13*, 35569–35582.

[26] Ghorbani‐Choghamarani, A., Tahmasbi, B., Noori, N., & Ghafouri‐nejad, R., *Journal of the Iranian Chemical Society*, **2017**, *14*, 681–693.

[27] Darabi, M., Nikoorazm, M., & Tahmasbi, B. *Inorganic Chemistry Communications*. **2025**, 114454.

[28] Nikoorazm, M., Tahmasbi, B., Darabi, M., Tyula, Y. A., Gholami, S., Khanmoradi, M., & Koolivand, M. *Journal of Porous Materials*. **2024**, *31*(2), 511-526.

[29] Nikoorazm, M., Khanmoradi, M., & Mohammadi, M. *Applied Organometallic Chemistry*. **2020**, *34*(4), e5504.

[30] Ghfar, A. A., & Liu, X. (2024). *Journal of Inorganic and Organometallic Polymers and Materials*. **2024**, *34*(12), 5901-5914.

[31] Mohseni, E., Ghorbani-Choghamarani, A., Tahmasbi, B., & Norouzi, M. *RSC advances*. **2024**, *14*(23), 16269-16277.

[32] Maseer, M. M., Kikhavani, T., & Tahmasbi, B. (2024). *Nanoscale Advances*. **2024**, *6*(15), 3948-3960.

[33] Li, C., Han, W., Zhu, T., Liu, L., Zhao, Y., Luo, F., ... & Yang, M. *ACS Applied Nano Materials*. **2024**, *7*(4), 4401-4412.

[34] Purohit, S., Oswal, P., Bahuguna, A., Tyagi, A., Bhatt, N., & Kumar, A. (2024). *RSC advances*. **2024**, *14*(37), 27092-27109.

[35] Bora, T. J., Gour, N. K., Saikia, L., Bora, U., Hazarika, N., Kim, D., ... & Bania, K. K. *Applied Catalysis A: General*. **2025**, *691*, 120053.

[36] Gharanjik, A. A., Alinezhad, H., & Kiani, A. *Journal of Materials Science*. **2024**, *59*(19), 8169-8185.

[37] Suteewong, T., Sai, H., Hovden, R., Muller, D., Bradbury, M. S., Gruner, S. M., & Wiesner, U. *Science*. **2013**, *340*(6130), 337-341.

[38] Li, W., Yue, Q., Deng, Y., & Zhao, D. (2013). *Advanced Materials*. **2013**, *25*(37), 5129-5152.

[39] Mehmood, A., Ghafar, H., Yaqoob, S., Gohar, U. F., & Ahmad, B. (2017). *J. Dev. Drugs*. **2017**, *6*(02), 100174.

[40] Pal, N., & Bhaumik, A. (2015). *RSC Advances*. **2015**, *5*(31), 24363-24391.

[41] Han, Y., & Zhang, D. *Current Opinion in Chemical Engineering*. **2012**, *1*(2), 129-137.

[42] Singh, S., Kumar, R., Setiabudi, H. D., Nanda, S., & Vo, D. V. N. *Applied Catalysis A: General*. **2018**, *559*, 57-74.

View Article Online
DOI: 10.1039/D5NA00951K

[43] Zhang, F., Yan, Y., Yang, H., Meng, Y., Yu, C., Tu, B., & Zhao, D. *The Journal of Physical Chemistry B*. **2005**, *109*(18), 8723-8732

[44] Klimova, T., Esquivel, A., Reyes, J., Rubio, M., Bokhimi, X., & Aracil, J. *Microporous and Mesoporous Materials*. **2006**, *93*(1-3), 331-343.

[45] Tamoradi, T., Ghorbani-Choghamarani, A., & Ghadermazi, M. *Polyhedron*. **2019**, *157*, 374-380.

[46] Jabbari, A., Tahmasbi, B., Nikoorazm, M., & Ghorbani-Choghamarani, A. *Applied Organometallic Chemistry*. 2018, *32*(6), e4295.

[47] Polshettiwar, V., & Varma, R. S. (2010). *Green Chemistry*. **2010**, *12*(5), 743-754.

[48] Wight, A. P., & Davis, M. E. (2002). Design and preparation of organic− inorganic hybrid catalysts. *Chemical reviews*. **2002**, *102*(10), 3589-3614.

[49] Shylesh, S., Schünemann, V., & Thiel, W. R. *Angewandte Chemie International Edition*. **2010**, *49*(20), 3428-3459.

[50] Tahmasbi, B., Darabi, M., Moradi, P., Tyula, Y. A., & Nikoorazm, M. *Polyhedron*. **2024**, *258*, 117038.

[51] Hajjami, M., Ghorbani, F., & Yousofvand, Z. *Applied Organometallic Chemistry*. **2017**, *31*(12), e3843.

[52] Yousofvand, Z., Hajjami, M., Ghorbani, F., & Ghafouri-Nejad, R. *Journal of Porous Materials*. **2018**, *25*, 1349-1358.

[53] Aghavandi, H., Ghorbani-Choghamarani, A., & Mohammadi, M. *Polycyclic Aromatic Compounds*. **2023**, *43*(8), 7439-7455.

[54] Tahmasbi, B., Ghorbani-Choghamarani, A., & Moradi, P., *New Journal of Chemistry*, **2020**, *44*, 3717-3727.
[55] Tahmasbi, B., & Ghorbani-Choghamarani, A., *New Journal of Chemistry*, **2019**, *43*, 14485—14501.
[56] Zhang, W., Chen, X., Tang, T., Mijowska, E., *Nanoscale*, **2014**, *6*, 12884-12889
[57] Wang, K., Yang, L., Zhao, W., Cao, L., Sun, Z., & Zhang, F. (2017). *Green Chemistry*. **2017**, *19*(8), 1949-1957.

[58] Prabu, M., Manikandan, M., Kandasamy, P., Kalaivani, P. R., Rajendiran, N., & Raja, T. *ACS Omega 4.* **2019***, 3500–3507*.

[59] Molaei, S., Tamoradi, T., Ghadermazi, M., & Ghorbani-Choghamarani, A. (2018). *Polyhedron*. 2018, *156*, 35-47.

[60] Alazzawi, H. F., Salih, I. K., & Albayati, T. M. (2021). Drug delivery of amoxicillin molecule as a suggested treatment for covid-19 implementing functionalized mesoporous SBA-15 with aminopropyl groups. *Drug Delivery*. **2021**, *28*(1), 856-864.

[61] Molaei, S., Tamoradi, T., Ghadermazi, M., & Ghorbani-Choghamarani, A. (2019). *Applied Organometallic Chemistry*. **2019**, *33*(1), e4649.

[62] Tahmasbi, B., Moradi, M., &Darabi, M., *Nanoscale Advances*, **2024**, *6*, 1932–1944.
[63] Darabi, M., Nikoorazm, M., Tahmasbi, B., & Ghorbanm-Ghoghamarani, A. *Applied Organometallic Chemistry*. **2024**, *38*(4), e7392.

[64] Hajighasemi, Z., Nahipour, A., Ghorbani-Choghamarani, A., & Taherinia, Z. *Nanoscale Advances*. **2023**, *5*(18), 4925-4933.

[65] Mohammadi, M., & Ghorbani-Choghamarani, A., *New Journal of Chemistry*, **2020**, 44, 2919-2929.

View Article Online
DOI: 10.1039/D5NA00951K

[66] Heydarian, S., Tahmasbi, B., & Darabi, M., *Nanoscale Advances*, **2025**, 7, 4867-4875.

[67] Ziegler Jr, C.B., & Heck, R. F., *The Journal of Organic Chemistry*, **1978**, *43*, 2941-2946.

[68] Dieck, H., & Heck, R.F., *Journal of the American Chemical Society*, **1974**, *96*, 1133-1136.

[69] Jutand, A., 2010, The Mizoroki–Heck Reaction. Print ISBN: 9780470033944, Online ISBN: 9780470716076. DOI:10.1002/9780470716076

[70] Ghasemirad, M., Norouzi, M., & Moradi, P. *Journal of Nanoparticle Research*. **2024**, *26*, 14.

[71] Ghorbani-Choghamarani, A., Mohammadi, M., Hudson, R. H., & Tamoradi, T. *Applied Organometallic Chemistry*. **2019**, *33*(8), e4977.

[72] Neelgund, G. M., & Oki, A. *Applied Catalysis A: General*. **2011**, *399*(1-2), 154-160.

[73] Wang, C. A., Li, Y. W., Hou, X. M., Han, Y. F., Nie, K., & Zhang, J. P. *ChemistrySelect*. **2016** ,*1*(7), 1371-1376.

[74] Song, K., Liu, P., Wang, J., Pang, L., Chen, J., Hussain, I., ... & Li, T. *Dalton Transactions*. **2015**, *44*(31), 13906-13913.

[75] Niakan, M., Asadi, Z., & Masteri-Farahani, M. *Colloids and Surfaces A: Physicochemical and Engineering Aspects*. **2018**, *551*, 117-127.

[76] Oliveira, R. L., He, W., Gebbink, R. J. K., & De Jong, K. P. *Catalysis Science & Technology*. **2015**, *5*(3), 1919-1928.

[77] Fortea-Perez, F. R., Julve, M., Dikarev, E. V., Filatov, A. S., & Stiriba, S. E. *Inorganica Chimica Acta*. **2018**, *471*, 788-796.

View Article Online
DOI: 10.1039/D5NA00951K

Data Availability

"All data generated or analyzed during this study are included in this published article and Supporting Information."